

Nature of $60\mu\text{m}$ emission in 3C 47, 3C 207 and 3C 334

Ilse M. van Bemmell¹, Peter D. Barthel¹, and Min S. Yun²

¹ Kapteyn Astronomical Institute, P.O. Box 800, NL-9700 AV Groningen, The Netherlands

² NRAO VLA, P.O. Box 0, Socorro, NM, USA

Received date; accepted date

Abstract. We try to explain the unusually high far-infrared emission seen by IRAS in the double-lobed radio-loud quasars 3C 47, 3C 207 and 3C 334. High resolution cm–mm observations were carried out to determine their radio core spectra, which are subsequently extrapolated to the far-infrared in order to determine the strength of the synchrotron far-infrared emission. The extrapolated flux densities being considerably lower than the observed values, a significant nonthermal far-infrared component is unlikely in the case of 3C 47 and 3C 334. However, this component could be responsible for the far-infrared brightness of 3C 207. Our analysis demonstrates that nonthermal emission cannot readily account for the difference between quasars and radio galaxies in the amount of their far-infrared luminosity. On the other hand, a significant role for this mechanism is likely; full sampling of the mm-submm spectral energy distributions is needed to address the issue quantitatively.

Key words: Galaxies: active; Radio continuum: general; (Galaxies:) quasars: general; (Galaxies:) quasars: individual: 3C 47, 3C 207, 3C 334

Barthel & Hoekstra 1995). This would imply that the simple unification model does not hold or that the assumption of isotropic $60\mu\text{m}$ radiation is incorrect. In support of the latter, Pier & Krolik (1992) drew attention to moderate anisotropy effects in the thermal far-infrared radiation from optically thick tori surrounding AGN. Furthermore, Hoekstra, Barthel & Hes (1997) demonstrated that beamed nonthermal far-infrared radiation is not insignificant in radio sources having prominent nuclei, and that the $60\mu\text{m}$ differences might be attributed to a stronger, beamed, nonthermal component in the QSR class. Within the unified model framework, QSRs would – at decreasing angle to the line of sight – naturally lead into the radio-loud blazar class, objects in which the dominance of the beamed component is without doubt. Indeed, both blazars and core-dominated QSRs display a smooth, single component spectral energy distribution, extending from radio to X-rays, indicating that all continuum radiation is of synchrotron origin (Landau et al. 1986). This causes blazars and core-dominated QSRs to be the most luminous IRAS AGN (Impey & Neugebauer 1988).

IRAS detected three $z \sim 0.5$, lobe-dominated 3CR QSRs at $60\mu\text{m}$, which corresponds to $\approx 40\mu\text{m}$ emitted wavelength. Comparable radio galaxies were not detected – contrary to the expectation within the simple unification model. The QSRs, 3C 47, 3C 207, and 3C 334, have relatively bright radio cores and large double-lobed structures. Two of these, 3C 47 and 3C 334, had been observed to display superluminal motion – a clear sign of beamed emission (e.g., Zensus & Pearson 1987) – thus raising the suspicion that their far-infrared brightness could be (partly) due to a beamed non-thermal component.

The goal of the present research is to investigate to what extent (beamed) nonthermal radiation can account for the infrared emission in lobe-dominated QSRs. We have determined the cm–mm core spectra of 3C 47, 3C 207, and 3C 334 in order to assess their nonthermal $60\mu\text{m}$ radiation by means of extrapolation. Given the possibility of flaring submm components (observed in blazars – e.g., Brown et al. 1989) this research is a first attempt

1. Introduction

Thermal emission from cool circumnuclear dust is widely accepted as an important mechanism for producing far-infrared radiation in radio-quiet and radio-loud AGN (Sanders et al. 1986, Chini et al. 1989, Antonucci et al. 1990). This emission – provided isotropic – gives the opportunity to test the orientation unification model of radio-loud quasars (QSRs) and powerful radio galaxies (RGs) (Barthel 1989, Urry & Padovani 1995), since matched samples should yield similar far-infrared output for both classes. However, from IRAS observations it appears that QSRs are stronger $60\mu\text{m}$ emitters than Fanaroff & Riley class II RGs (Heckman et al 1992, 1994, Hes,

Send offprint requests to: bemmell@astro.rug.nl

source	3C 47	3C 207	3C 334
name (B1950)	0133+207	0838+133	1618+177
z	0.425	0.684	0.555
S_{60} (mJy)	206	114	126
$\log P_{178}$ (W/Hz)	28.36	28.50	28.21
$\log P_5^c$ (W/Hz)	25.68	26.94	26.10
R_5	0.05	0.28	0.15(var.)
$\log L_{60}$ (W)	38.98	39.16	39.01
v_{SLM}	7.4c	suspected	3.2c

Table 1. Basic properties of the quasars. S_{60} is the IRAS flux density at 60 μ m, P_{178} is the total radio source power at 178 MHz (calculated adopting a spectral index of 0.7), P_5^c is the 5 GHz core radio power, R_5 is the core/total flux density ratio at 5 GHz emitted frequency, calculated adopting radio spectral indices of 0 and 0.7 for the core and extended emission respectively.

to isolate nonthermal and thermal FIR radiation. Observations over a wider frequency range are forthcoming.

2. Sample description, observations and data reduction

In order to determine the synchrotron far-infrared component in 3C 47, 3C 207, and 3C 334, we observed their cm-mm core spectral energy distribution, using the NRAO Very Large Array and the Owens Valley Radio Observatory mm-array. We supplemented these data with VLA Archive and literature data, to examine core variability. Some characteristics¹ of the three quasars are listed in table 1. The parameter R_5 specifies the fractional core flux density at 5 GHz emitted frequency. It should be noted that double-lobed 3C narrow-line radio galaxies of similar radio power have typical R_5 -values of order 0.01 (e.g., Ferri et al. 1997). As mentioned above, 3C 47 and 3C 334 are reported superluminal objects (Vermeulen et al. 1993, Hough et al. 1992), while 3C 207 is a suspected superluminal object (Hough, 1984). The last entry in table 1 specifies the measured superluminal component speeds. Images of the global QSR radio morphologies can be found in Bridle et al. (1994 – 3C 47 and 3C 334) and Bogers et al. (1994 – 3C 207). They all show large double-lobed structures and fairly prominent one-sided jets.

2.1. VLA cm observations

VLA A- and A/B-array observations at 4.9 GHz (C-band, 6 cm), 8.4 GHz (X, 3.6 cm), 15 GHz (U, 2 cm), 22 GHz (K, 1.2 cm) and 43 GHz (Q, 7 mm), were conducted 1995 Sept. 5, 6, 7. Two IFs were recorded at 50 MHz bandwidth each. Resolving VLA beams varied from 0.9 to 0.2 arcsec, at C- down to K-band. Q-band resolution was 0.4 arcsec, due the fact that only the six inner telescopes of the array

¹ We use throughout $H_0 = 50 \text{ km sec}^{-1} \text{ Mpc}^{-1}$, $q_0 = 0.5$

ν (GHz)	3C 84	3C 286
4.9	27.63	7.426
8.4	23.83	5.206
15	23.63	3.502
22	19.75	2.554
43	12.47	1.472

Table 2. Input flux densities in Jy of the primary calibrators – see text

were equipped with Q-band receivers. High resolution observations are necessary in order to isolate core from possible jet emission. Single 3 minute snapshot scans were made at C- and X-band, two scans of 3.5 minutes each at U- and K-band, and three 3.5 minute scans at Q-band. Beam reference pointing at Q-band was employed. Secondary phase and amplitude calibrators were observed before and after each scan.

Primary calibrators were 3C 84 and 3C 286, with appropriate baseline constraints, and inferred/adopted flux densities as listed in table 2. Both primary calibrators were observed during the run on 3C 207 in order to infer the absolute 3C 84 flux density scale (3C 84 was used as primary calibrator for the 3C 47 observations). Calibration uncertainty is dominated by the uncertainty in the absolute flux density of the primary calibrators, which is $\approx 1\%$. The array performed well: antenna phase and amplitude calibration appeared stable to within $\approx 0.1\%$, except for Q-band where these figures were $\approx 1\%$.

Data reduction was carried out in Groningen, using standard AIPS routines. The IF1 data being of inferior quality, analysis was restricted to the IF2 data. Tapering was applied for the (high resolution) high frequency data, aiming for comparable resolution at all bands. All cores were detected, except for 3C 47 in K- and Q-band, and 3C 334 in Q-band. For these we derived an upper limit, using the noise levels. The 3C 47 K-band map was dominated by large phase errors and therefore only a fairly high upper limit could be determined. The noise in all maps, including the calibrators, was on the order of one to a few mJy/beam, except for Q-band, where it was about 6 mJy/beam for 3C 47 and 3C 207. Few Q-band antenna’s were available for the 3C 334 observations, yielding a low quality image and high Q-band flux density upper limit. We use the dirty map 5σ level as Q-band upper limit. Gaussian core profiles were fitted to determine the integral flux densities, using the AIPS routine IMFIT. The resulting values are listed in table 3. The (3σ) errors combine calibration and fitting uncertainties.

2.2. OVRO 3mm observations

Aperture synthesis observations of the 100 GHz continuum emission in 3C 47, 3C 207, and 3C 334 were carried out with the Owens Valley Millimeter Array on Septem-

ν (GHz)	3C 47	3C 207	3C 334
4.9	77.9 \pm 3	532 \pm 21	159.5 \pm 6
8.4	67.1 \pm 3	648 \pm 26	173 \pm 7
15	50.4 \pm 2	744 \pm 30	180 \pm 7
22	\leq 42	726.5 \pm 29	143.5 \pm 6
43	\leq 30	701.5 \pm 35	\leq 60

Table 3. VLA core flux density values in mJy from Gaussian model fits

ber 22, 1995, hence nearly simultaneously with the VLA observations. There were six 10.4 m diameter telescopes in the array, each equipped with an SIS receiver cooled to 4K. The receivers were tuned to 100 GHz, and typical system temperatures of 300K (single sideband) were achieved. The array was in a compact configuration with baselines of 15–65m E-W and 15–35m N-S, yielding a typical beam size of 14''(N-S) \times 6''(E-W). An analog correlator with 1 GHz total bandwidth was used for these continuum mode observations. Nearby quasars were observed at 20 minute intervals to track the phase and short term instrument gain, and Uranus ($T_B=120$ K) was used for the absolute flux calibration. The data were calibrated using the standard Owens Valley array program MMA (Scoville et al. 1993), while DIFMAP (Shepherd et al. 1994) and AIPS were used for mapping and analysis. The uncertainty in the absolute flux measurement is about 15%, and the positional accuracy of the resulting images is better than $\sim 0.5''$.

A 100 GHz nuclear continuum source is detected in all three quasars, unresolved by the synthesized beam (see table 4). The on-source integration time was between 180 and 340 minutes, resulting in noise sensitivity of 1–2 mJy/beam. 3C 207 is a strong source at 100 GHz, and the synthesized map is limited by dynamic range rather than by thermal noise. Evidence for lobe structures is seen in the visibility plots for all three sources, but limited uv -coverage did not permit mapping of these structures. In 3C 47, two bright hot spots (features A and H in Bridle et al. 1994) are clearly detected, located $\sim 30''$ away from the core. However, their fluxes are uncertain because they lie near the half-power point of the primary beam. Contamination with arcsec scale jet emission at 100 GHz is negligible, due to the spectral steepness of jet radiation combined with the fact that the elongated synthesized beam will not pick up substantial jet emission, as these are not oriented N-S.

2.3. Archive and literature data

Archival VLA data (1982–1983) were obtained from projects by Wardle, Perley, and Ekers. These data were reduced in the same way as our 1995 data. To check for, and exclude, calibration induced variability, we compared the

source	$S_{100\text{GHz}}$
3C 47	16.3 \pm 0.9
3C 47 N.hotspot	6.8 [†] \pm 0.9
3C 47 S.hotspot	15.4 [†] \pm 0.9
3C 207	512 \pm 7
3C 334	37.1 \pm 1.9

[†] not corrected for primary beam attenuation.

Table 4. OVRO 100 GHz core flux densities (mJy)

source	observer	array	ν (GHz)	F
3C47	Ekers	C	4.9	71 \pm 3
3C207	Wardle	A	4.9	477 \pm 19
3C207	Wardle	C	15	672 \pm 27
3C334	Perley	C	4.9	165 \pm 7
3C334	Perley	C	15	99 \pm 4
3C334	Perkey	C	22	54 \pm 3

Table 5. Arrays, bands and flux densities in mJy from VLA archive data – see text for details.

archive short spacing flux densities with our 1995 values. Details on the observations and flux densities are listed in table 5.

In addition to the archive VLA data, we examined literature data from other telescopes, in search for variability during the epoch 1975–1995. These observations are listed in table 6. Since for a number of observations no precise value for the resolution is given, we listed the telescopes used and whenever possible in which configuration.

3. Results and spectral fits

3.1. Core cm–mm spectra

The core spectra for 3C 47, 3C 207 and 3C 334 are plotted in figure 1, using data from tables 3, 4, 5, and 6. Our 1995 data, which will be used for the spectral energy distribution (SED) fits, are plotted as open circles. The unusually high IRAS 60 μ m points appear on the right in each figure as filled circles. Literature data are plotted as stars, the 1982/1983 VLA archive data as filled triangles. All errors are within the sizes of the points. The following remarks can be made for the individual objects.

3.1.1. 3C 47

An archival VLA 5 GHz dataset (observed by Ekers in June 1982, C array) appeared in good agreement with our observations: no evidence for core variability is seen. Also the literature data show no sign of cm variability over the last twenty years. Since this quasar seems to have a stable core, we decided to include the 1.4 GHz datapoint (1985

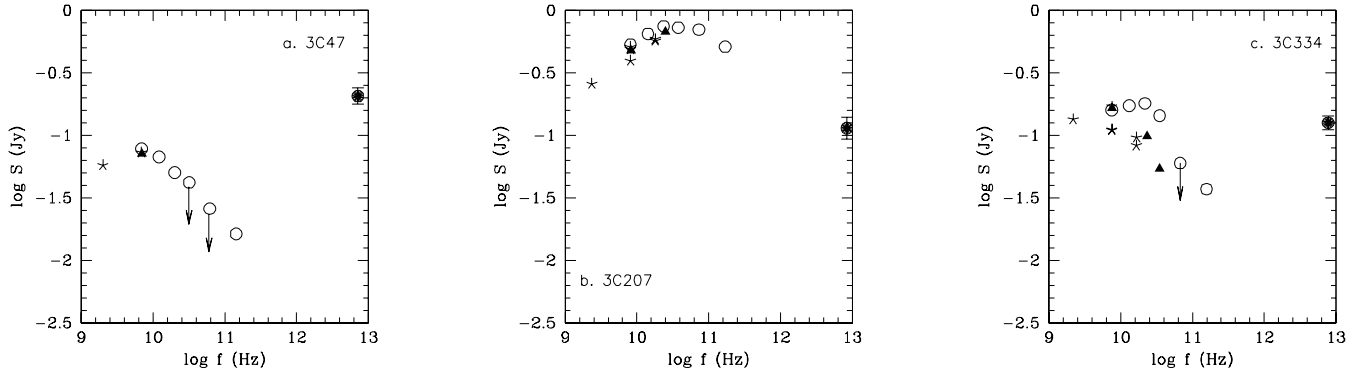


Fig. 1. Rest frame core spectra for the IRAS detected quasars, including literature and 1983 VLA data. Open circles represent our 1995 data, filled triangles 1983 VLA data, and stars literature data. The filled circles represent the total (thermal plus nonthermal) IRAS 60 μ m flux densities. All error bars fall within the size of the points, except for the IRAS observations.

source	ν (GHz)	F	Ref.	Resolution	Year
3C 47	1.4	57.7	1	VLA B+C	85/86
3C 47	4.8	72.8	1	VLA A+B	85/86
3C 207	1.4	258	9	VLA A	92
3C 207	4.8	395	4	VLA	80
3C 207	5	510	2	MRAO ^a	74 ^b
3C 207	5	490	3	transatl.VLBI	81
3C 207	10.6	570	4	VLA	80
3C 207	10.6	588	10	VLA	86 ^b
3C 334	1.4	134	8	VLA A	80/81
3C 334	4.9	138	6	VLA A+B	86
3C 334	5	170	7	MRAO	77 ^b
3C 334	5	110	3	transatl.VLBI	81
3C 334	10.6	83	5	transatl.VLBI	83
3C 334	10.6	96	5	transatl.VLBI	88

^a MRAO (Cambridge, UK) 5 km telescope

^b date of publication

Table 6. Literature references, with year of observation. All fluxes are in mJy; column 4 gives the literature reference. References: 1=Fernini et al. (1991); 2=Pooley & Henbest (1974); 3=Barthel et al. (1984); 4=Rudnick et al. (1986); 5=Hough et al. (1992); 6=Bridle et al. (1994); 7=Jenkins et al. (1977); 8=Hintzen et al. (1983); 9=Bogers et al. (1994); 10=Hough (1986).

observation, VLA A-array) from Fernini et al. (1991) in our fitting procedure.

3.1.2. 3C 207

For this source we retrieved VLA archive observations at C- and U-band, made by Wardle in March 1982 (A-array) and May 1983 (C-array) respectively. The core flux densities are in good agreement with our 1995 VLA data. Also, most literature data show no large discrepancies with respect to our data. However, Hough (1986) reports changes of $\sim 100 - 200$ mJy in the early 1980's. Comparison of transatlantic VLBI with VLA data at 5 GHz is also indicative of some level of variability in the 3C 207 nucleus. Since the core shows no strong variability, we added the (1992 VLA A-array) 20 cm flux density value from Bogers et al. (1994).

3.1.3. 3C 334

An extensive archival VLA data set was available for this quasar, observed by Perley in January 1983 (C-array). Observations were carried out in C-, U-, and K-band. 3C 334 displays substantial core variability with respect to our 1995 data, as seen from figures 1 and 3. Figure 3 displays 5 GHz core flux density values, measured at $\sim 0.5''$ resolution over the last two decades (data from table 2 in Hough et al. 1992).

3.2. Core spectral energy distributions

To obtain a good estimate of the (beamed) nonthermal 60 μ m flux density, we fitted curves to the nearly simultaneous 1995 cm and mm data. As mentioned above, for 3C 47 and 3C 207 we added the 20cm (L-band) points from Fernini et al. (1991) and Bogers et al. (1994) respectively. Upper limits are excluded from the fitting procedure.

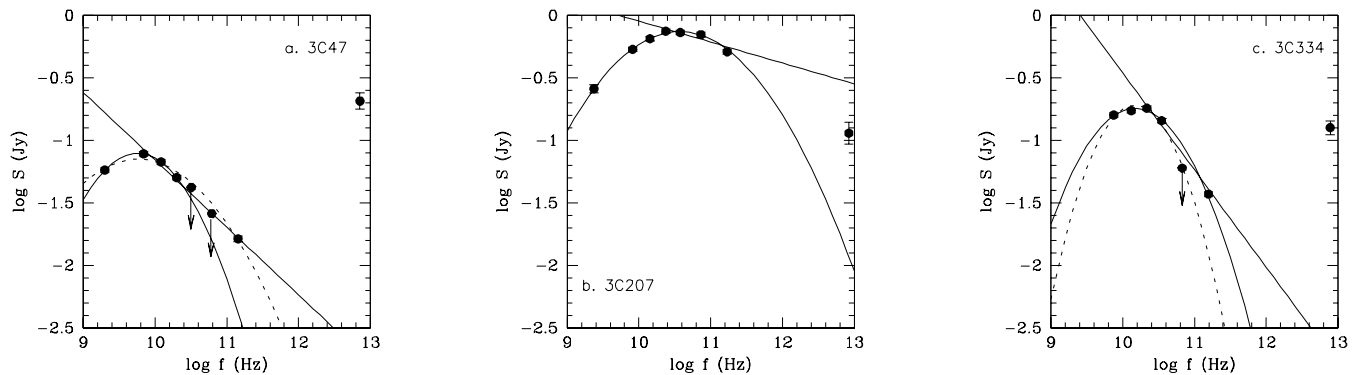


Fig. 2. Rest frame fits for the IRAS detected quasars, using only our 1995 data and additional 20cm points for 3C 47 and 3C 207. The straight lines represent powerlaw fits to the high frequency points, the parabola fits draw from an empirical result for blazar spectra. The dashed parabola in figure a includes the 3mm point, while the solid parabola does not. See text for details on the fitting procedure.

dures. The fitted curves can subsequently be extrapolated into the far-infrared. However, the shape of the curve is a priori unknown. We therefore used two different models. First we fitted a parabola, which is an empirical result for blazar spectra (Landau et al., 1986). In the light of the unification theory and provided we are dealing with single components, these parabolic fits can be used to fit core spectra for double-lobed quasars. It should be noted however that Brown et al. (1989) found evidence for double components in their blazar sample. We will come back to this issue in section 4.1.

Second we used the theoretical spectrum of a single self-absorbed synchrotron source, which has a $F \sim \nu^\alpha$ powerlaw at frequencies larger than the turnover frequency. For this fit we excluded all the frequencies below the turnover frequency. Both fits were done using least-squares methods. The resulting fits, in the QSR rest frames, are shown in figure 2. With the exception of 3C 47, the parabolae fit remarkably well, but it should be kept in mind that their high frequency parts are not well constrained.

Given the upper limits at 1cm and 7mm, a parabola does not yield a good fit to the 3C 47 data when we include the 3mm point (dashed parabola in figure 2a). Leaving out this 3mm point, a single parabola does fit the 3C 47 data remarkably well (solid parabola in figure 2a). A secondary (sub)mm component may be causing the rather high 3mm point. In the case of 3C 334, the parabola does fit well (solid parabola in figure 2c), but the Q-band upper limit is below our fit. If we exclude the 3mm point from the fit procedure, the parabola does not change significantly.

source	S_{60}	$F_{e,par}^a$	$F_{e,pl}^b$	ΔF_{60}
3C 47	206 ± 33	~ 0	2.0 ± 0.1	~ 204
3C 207	114 ± 26	11.5 ± 0.1	291 ± 5	≥ -177
3C 334	126 ± 17	~ 0	1.9 ± 0.1	~ 124

^a extrapolated flux density from parabola fit

^b extrapolated flux density from powerlaw fit

Table 7. Comparison of measured total and extrapolated non-thermal FIR flux densities, in mJy.

The dashed parabola is a fit including the Q-band upper limit and excluding the 3mm point.

As can be seen immediately, only in 3C 207 the IRAS flux density may suffer from substantial nonthermal contamination, adopting the high frequency powerlaw fit. For the other two quasars the far-infrared point is far above the extrapolated nonthermal value, leaving a factor of 100 to account for. Note that especially 3C 47 stands out: the IRAS point is even higher than the radio peak flux density. The extrapolated values of the FIR flux density for different models are compared with the observed values in table 7. S_{60} is the IRAS flux density from Hes et al. (1995), F_e are the extrapolated flux densities and ΔF_{60} is the FIR excess defined as the difference between observations and models at 60 μ m observed wavelength. All values are in mJy/beam.

4. Analysis and discussion

Since there is a substantial time interval between the (1983) IRAS observations and the other data, core vari-

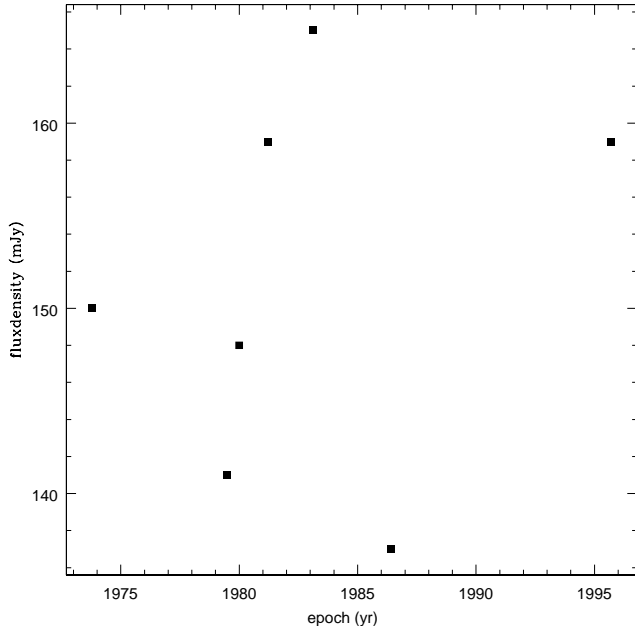


Fig. 3. Variability of 3C 334 over the last two decades. Data points taken from table 2 in Hough et al. (1992)

ability could be a possible explanation for the FIR excess. However, long-term radio data from literature show that the core variations do not exceed $\approx 10\%$ and therefore are not large enough to explain the total excess. In addition, all variability references report fairly low core flux densities for 1983 (IRAS epoch), which does not help to explain a FIR *excess*. Although the IRAS detections could be spurious, since the sources are close to the detection limit, or due to a confusing source, the issue remains why no spurious radio galaxy detections appear. Below we examine all possible explanations for the FIR excess observed in these quasars.

4.1. Non-thermal FIR

The main goal of this research was to find out if beamed non-thermal radiation could be responsible for the FIR excess. Adopting single component core models it is evident from the plots in figure 2 that beaming cannot be responsible, except for 3C 207 applying the powerlaw fit. However, we do know that beaming operates in 3C 47 and 3C 334, both superluminal objects. Both the FIR beaming and the radio core R-parameter depend on the Doppler factor Γ to some power. In terms of R-parameter strength the strongest component of nonthermal FIR radiation would be expected from 3C 207, followed by 3C 334 and 3C 47. This order is not reflected in the total 60 μ m luminosi-

ties: the largest FIR excess, normalized with respect to the 5 GHz flux density, originates in the quasar with the smallest core fraction. While the reported superluminal velocities roughly scale with the infrared excess in 3C 334 and 3C 47, a measurement is still lacking in 3C 207. Moreover, these tests have little statistical significance.

The formula derived by Hoekstra et al. (1997) permits an estimate of the relative amount of beamed radiation. Hoekstra et al. use a relation depending on Q and C_{60} to estimate the amount of beamed 60 μ m emission. Here Q is the observed 5GHz core fraction, and C_{60} is a measure for the value of Q at which beaming becomes significant. They determined the value of C_{60} from a large sample of FIR-detected blazars and quasars, including the three discussed here. This yields a maximum nonthermal FIR contribution of 15%, for 3C 207, and considerably less for 3C 47 and 3C 334.

The Hoekstra et al. (1997) analysis postulates a direct (single component) connection between the nonthermal radio and FIR emission. It is quite likely that the real situation is more complicated. As mentioned above, Brown et al. (1989) demonstrated the presence of two nonthermal core components in blazars. One component is fairly quiescent and dominates the radio to mm region. A second, ultracompact, component is prevalent in the submm regime. This component becomes self-absorbed at wavelengths longer than ~ 3 mm, and displays strong variability (flares), sometimes within days. Our data do not constrain the submm region well: it is likely that such variable submm components are being missed in our analysis. The possibility that such a component has pushed the total (thermal plus nonthermal) FIR into IRAS detection cannot as yet be ruled out. In fact, as inferred from the 100 GHz data, our 3C 47 observations may have caught such a submm component. In 3C 334 this might also be the case, considering that our Q-band upper limit is lower than the predicted value if we include the 3mm point in our fit.

We stress that since the IRAS detections are just above the detection limit, not the total 60 μ m emission has to be accounted for, but only a substantial nonthermal component lifting the total 60 μ m flux into IRAS detection. For 3C 47 and 3C 334, superluminal and hence beamed objects, the possibility of an additional, variable submm component is considered likely. Full sampling of the cm-mm-submm-FIR spectral range is needed to confirm our suspicion.

4.2. Thermal FIR

If most or all 60 μ m emission is identified with thermal radiation, the question arises why 3C 47, 3C 207 and 3C 334 are more luminous than other quasars and radio galaxies. There are several mechanisms that can produce thermal FIR in AGN: cold cirrus and warm starburst heated dust in the host galaxies, and furthermore warm AGN-related

dust. Models for these components are for instance described by Rowan-Robinson & Crawford (1989). In order to distinguish between these, more IR data are needed to perform a detailed analysis of the FIR spectral energy distribution. Multiple component fitting is necessary to isolate the various dust components. However, if these mechanisms are responsible for the FIR excess, unification is difficult, since it states that radio galaxies and lobe-dominated quasars are basically the same objects and thus should have similar dust composition.

If we wish to maintain the unification concept we have to postulate optically thick dust emission at $\sim 40\mu\text{m}$ in combination with aspect effects. If the FIR excess originates from an optically thick torus shielding the optical QSO in a plane perpendicular to the radio axis, models by Pier & Krolik (1992) yield aspect dependent anisotropies of factors up to about ten. At longer FIR wavelengths the anisotropies should become zero (optical thin dust): data at 100 μm or longer wavelengths are needed to investigate optical thickness effects.

5. Conclusions and future research

We cannot readily explain the extraordinary high FIR flux density observed in the 3C 47, 3C 207, and 3C 334. While relativistic beaming of a single nonthermal component cannot account for the total FIR radiation, the radiation of relativistically beamed multiple core components is likely to contribute significantly in the far-infrared. Thermal mechanisms could play a role, in combination with optical thickness and aspect effects, but we need more data in the submm and infrared to address these in detail. We are currently engaged in measurements of matched pairs of radio galaxies and quasars, comparing their thermal FIR output by combining cm, mm, submm and FIR data from VLA, JCMT, and ISO observations. In the meantime, we have little doubt that the importance of nonthermal FIR and submm radiation in double-lobed radio sources has been underestimated.

Acknowledgments We acknowledge initial involvement in this work of R. Hes and H. Hoekstra, OVRO support by N. Scoville and A. Sargent, and the use of archival VLA data from R. Ekers, R. Perley, and J. Wardle. The NRAO VLA is operated by Associated Universities, Inc. under contract with the National Science Foundation. OVRO research is supported in part by NSF Grant AST 93-14079.

References

Antonucci, R., Barvainis, R., Alloin, D., 1990, ApJ, 353, 416
 Barthel, P.D., Miley, G.K., Schilizzi, R.T., Preuss, E., 1984, A&A, 140, 399
 Barthel, P.D., 1989, ApJ, 336, 606
 Bogers, W.J., Hes, R., Barthel, P.D., Zensus, J.A., 1994, A&AS, 105, 91

Bridle, A.H., Hough, D.H., Lonsdale, C.J., Burns, J.O., Laing, R.A., 1994, AJ, 108, 766
 Brown, L.M.J., Robson, E.I., Gear, W.K., et al., 1989, ApJ, 340, 129
 Chini, R., Biermann, P.L., Kreysa, E., Gemünd, H.-P., 1989, A&A, 221, L3
 Fernini, I., Burns, J.O., Leahy, J.P., Basart, J.P., 1991, ApJ, 381, 63
 Fernini, I., Burns, J.O., Perley, R.A., 1997, AJ, 114, 2292
 Heckman, T.M., Chambers, K.C., Postman, M., 1992, ApJ, 391, 39
 Heckman, T.M., O’Dea, C.P., Baum, S.A., Laurikainen, E., 1994, ApJ, 428, 65
 Hes, R., Barthel, P.D., Hoekstra, H., 1995, A&A, 303, 8
 Hintzen, P., Ulvestad, J., Owen, F., 1983, AJ, 88, 709
 Hoekstra, H., Barthel, P.D., Hes, R., 1997, A&A, 319, 757
 Hough, D.H., 1984, private communication
 Hough, D.H., 1986 PhD thesis, California Institute of Technology
 Hough, D.H., Readhead, A.C.S., Wood Jr, D.A., Feldmeier, J.J., 1992, ApJ, 393, 81
 Impey, C.D., Neugebauer, G., 1988, AJ, 95, 307
 Jenkins, C.J., Pooley, G.G., Riley, J.M., 1977, MemRAS, 84, 61
 Landau, R., Golisch, B., Jones, T.J., et al., 1986, ApJ, 308, 78
 Pier, E.A., Krolik, J.H., 1992, ApJ, 401, 99
 Pooley, G.G., Henbest, S.N., 1974, MNRAS, 169, 477
 Rowan-Robinson, M., Crawford, J., 1989, MNRAS, 238, 523
 Rudnick, L., Jones, T.W., Fiedler, R., 1986, AJ, 91, 1011
 Sanders, D.B., Phinney, E.S., Neugebauer, G., Soifer, B.T., Matthews, K., 1989, ApJ, 347, 29
 Scoville, N.Z., Carlstrom, J.E., Chandler, C.J., et al., 1993, PASP, 105, 1482
 Shepherd, M.C., Pearson, T.J., Taylor, G.B., 1994, BAAS, 26, 987
 Urry, C.M., Padovani, P., 1995, PASP, 107, 803
 Vermeulen, R.C., Bernstein, R.A., Hough, D.H., Readhead, A.C.S., 1993, ApJ, 417, 541
 Zensus, J.A., Pearson, T.J., eds. 1987, Superluminal Radio Sources, Cambridge Univ. Press